TECHNICAL NOTES

NATIONAL ADVISORY COMMITTEE FOR AERONAUTICS

No. 834

THE CALCULATION OF SPAN LOAD DISTRIBUTIONS ON SWEPT-BACK WINGS

By William Mutterperl
Langley Memorial Aeronautical Laboratory

Washington
December 1941

NATIONAL ADVISORY COMMITTEE FOR AERONAUTICS

TECHNICAL NOTE NO. 834

THE CALCULATION OF SPAN LOAD DISTRIBUTIONS ON SWEPT-BACK WINGS

By William Mutterperl

SUMMARY

Span load distributions of swept-back wings have been calculated. The method used was to replace the wing with a bound vortex at the quarter-chord line and to calculate the downwash due to the system of bound and trailing vortices to conform at the three-quarter-chord line to the slope of the flat-plate wing surface. Results are given for constant-chord and 5:1 tapered plan forms, for sweepback angles of 0°, 30°, and 45°, and for aspect ratios of 3, 6, and 9. Some comments on the stalling of swept-back wings are included.

INTRODUCTION

Airplane designs are often proposed in which stability and control are provided by a wing with a large angle of sweepback instead of by the conventional fuselage and tail arrangement. The calculation of the aerodynamic forces is more difficult on such a wing than on the corresponding unswept-back wing because of the more complicated nature of the vortex system, the flow of which is to be calculated. The problem is essentially that of two yawed airfoils (the two halves of the swept-back wing) subject not only to the effects of finite aspect ratio but also to their mutual interference.

Wieghardt has shown in his work with rectangular flat plates (reference 1) that good accuracy in the total lift force can be attained by replacing the plate with a bound vortex at the quarter-chord line and making the downwash due to the bound vortex and its associated trailing vortex system conform, at the three-quarter-chord line, to the slope of the flat plate.

Such a procedure is rigorously correct for an unyawed,

rectangular flat plate of infinite span. The method also holds for a yawed, infinite-span flat plate because, in this case, the spanwise component of the free-stream velocity has no effect (if potential flow is assumed) on the lift whereas the component normal to the span has the same effect as on an unyawed airfoil. More precisely, let the airfoil be yawed through an angle Λ at zero angle of attack and then rotated through an angle α about the line with respect to which Λ was measured. If the free-stream velocity V is resolved along the three mutually perpendicular directions - namely, spanwise, chordwise perpendicular to the span, and normal to the plane of the flat plate - the velocity components are, respectively, $V \sin \Lambda \cos \alpha$, $V \cos \Lambda \cos \alpha$, and $V \sin \alpha$. Inasmuch as the chord measured normal to the span is $c_0 \cos \Lambda$, then from two-dimensional thin-airfoil theory, the circulation Γ is given by

$$\Gamma = \pi V c_0 \cos \Lambda \sin \alpha \tag{1}$$

Also, from two-dimensional wing theory, the center of pressure of the lift forces is at the quarter-chord line. If a bound vortex of circulation given by equation (1) is placed at the quarter-chord line, the normal induced velocity w at the three-quarter-chord line is

$$w = \frac{\Gamma}{2\pi r} = \frac{\pi V c_0 \cos \Lambda \sin \alpha}{2\pi \frac{c_0}{2} \cos \Lambda}$$

or

$$w = V \sin \alpha \tag{2}$$

which is exactly the amount needed to produce a resultant flow along the flat-plate equivalent of the thin airfoil at the three-quarter-chord point.

The extension of Wieghardt's method to flat plates of swept-back plan form has been made in the present paper. A swept-back bound vortex was placed at the quarter-chord line (fig. 1) and the downwash due to the bound vortex and its trailing-vortex system was calculated at points on the three-quarter-chord line. The bound vortex strength was determined by the condition that the resultant flow at the three-quarter-chord line be tangent to the flat plate. The span load distribution thus determined should be expected to be less valid near the tips and the center of the

wing than in between. In the center, the effect of one wing upon the other is strong and the bound vortices are curved lines rather than broken lines; whereas, at the tips, the presence of strong trailing vortices invalidates the argument of the previous paragraphs, which was based on two-dimensional wing theory.

The results obtained for the flat-plate wing surfaces may be applied to wings having the usual type of airfoil section on the assumption that the finite thickness and camber of the wing do not appreciably displace the vortex system from the horizontal plane. Furthermore, inasmuch as the section lift-curve slope a_0 generally differs from 2π, the airfoil chord to be used with the results of this paper is

$$c = \frac{a_0}{2\pi} c_{actual}$$

This correction is based on the two-dimensional airfoil relation

$$\Gamma = \frac{1}{2} ca_0 V\alpha$$

in which ca_0 occurs as a product. The value of a_0 will depend on the angle of sweepback Λ as well as on the airfoil section. If there were no viscosity effects nor trailing-vortex system, a_0 would be determined by the section perpendicular to the span because the component of the air flow perpendicular to the span produces the lift. The chief cause of the reduction in a_0 from its theoretical value as given by potential theory is, however, the viscosity phenomena (boundary layer, separation, etc.) that depend on the actual path of the air particles over the airfoil. Because, for large aspect ratio at least, the streamlines over the airfoil do not greatly depart from the free-stream direction, the slope of the lift curve of the airfoil section in the free-stream direction should be used.

SYMBOLS

The following symbols are used:

b wing span, measured along quarter-chord line from tip to tip

s wing semispan $(b/2)$

Λ sweepback angle, measured from quarter-chord line

α angle of attack, measured in free stream direction

S area of plan form of wing

c wing chord measured in free-stream direction

c_0 wing root chord measured in free-stream direction

A aspect ratio $\left(\frac{b^2 \cos^2 \Lambda}{S}\right)$

L total lift

a_0 slope of section lift curve

C_L lift coefficient $\left(\frac{L}{\frac{1}{2} \rho V^2 S}\right)$

l lift per unit length along span

Γ circulation

D_i induced drag

C_{D_i} induced-drag coefficient $\left(\frac{D_i}{\frac{1}{2} \rho V^2 S}\right)$

ρ density of air

V free-stream air velocity

w induced downwash velocity

Coordinates:

η coordinate of downwash point in direction of quarter-chord line (positive to right)

σ coordinate of bound vortex element in direction of quarter-chord line (positive to right)

$\bar{\sigma}$ center of pressure of span load distribution

ϕ angle corresponding to σ ($\cos \phi = \sigma/s$)

ψ angle corresponding to η ($\cos \psi = \eta/s$)

y perpendicular to free-stream direction in plane of wing (positive to right)

Subscripts:

\+ refers to right side of wing

\- refers to left side of wing

1 refers to bound vortex

2 refers to trailing vortex

METHOD

The flat-plate wing surface of swept-back plan form is replaced with a bound vortex at the quarter-chord line (fig. 1). The bound vortex and an element of the trailing-vortex sheet, as well as the symbols used in the following expressions, are shown in figure 1. By the Biot-Savart law the induced velocity w (positive downward) at the point P on the three-quarter-chord line, due to the bound vortex Γ on the quarter-chord line, is

$$w_1 = \frac{1}{4\pi}\int_0^s \frac{\Gamma \sin \theta_+ \, d\sigma_+}{r_+^2} + \frac{1}{4\pi}\int_{-s}^0 \frac{\Gamma \sin \theta_- \, d\sigma_-}{r_-^2} \tag{3}$$

which, upon substitution of the geometrical relations

$$\left.\begin{aligned} \cos \theta_+ &= \frac{\sigma_+ - \eta_+ - B_+ \tan \Lambda}{r_+} \qquad \sin \theta_+ = \frac{B_+}{r_+} \\ \cos \theta_- &= \frac{\sigma_- - \eta_- + B_- \tan \Lambda}{r_-} \qquad \sin \theta_- = \frac{B_-}{r_-} \end{aligned}\right\} \tag{4}$$

becomes

$$4\pi w_1 = -\frac{1}{B_+}\int_{\theta_{+o}}^{\theta_{+s}} \Gamma\,(\theta_+)\,\sin\,\theta_+\,d\theta_+$$

$$-\frac{1}{B_-}\int_{\theta_{-s}}^{\theta_{-o}} \Gamma(\theta_-)\,\sin\,\theta_-\,d\theta_- \qquad (5)$$

The corresponding expression for the trailing vortex sheet is

$$4\pi w_2 = -\int_0^s \frac{\left[1 - \cos\left(\theta_+ - \Lambda + \frac{\pi}{2}\right)\right] d\Gamma}{\sigma_+ \cos\,\Lambda - y}$$

$$-\int_{-s}^{0} \frac{\left[1 + \cos\left(\theta_- + \Lambda - \frac{\pi}{2}\right)\right] d\Gamma}{\sigma_- \cos\,\Lambda - y} \qquad (6)$$

The total induced velocity is the sum of equations (5) and (6); this sum becomes, after equation (5) is integrated by parts and it is noted that Γ is zero at the wing tips,

$$4\pi w = -\frac{\Gamma(\theta_{+o})\,\cos\,\theta_{+o}}{B_+} + \frac{\Gamma(\theta_{-o})\,\cos\,\theta_{-o}}{B_-} - \frac{1}{B_+}\int_0^s \cos\,\theta_+\,d\Gamma$$

$$-\frac{1}{B_-}\int_{-s}^{0} \cos\,\theta_-\,d\Gamma - \int_c^s \frac{[1 + \sin\,(\theta_+ - \Lambda)]}{\sigma_+ \cos\,\Lambda - y}\,d\Gamma$$

$$-\int_{-s}^{0} \frac{1 + \sin\,(\theta_- + \Lambda)}{\sigma_- \cos\,\Lambda - y}\,d\Gamma \qquad (7)$$

The variables of integration σ, θ, and Γ may be expressed in terms of a single independent variable ϕ, varying continuously from 0 to π across the span from right to left. Thus by the definition

$$\sigma_- = s \cos \phi \quad \text{for} \quad -s \leq \sigma_- \leq 0$$

$$\sigma_+ = s \cos \phi \quad \text{for} \quad 0 \leq \sigma_+ \leq s \tag{8}$$

and the geometric relation

$$\tan \theta_+ = \frac{B_+}{\sigma_+ - A_+} \tan \theta_- = \frac{B_-}{\sigma_- - A_-} \tag{9}$$

together with the usual Fourier series expression for Γ

$$\Gamma = 4\pi V c_0 \sin \alpha \sum_{k=0}^{\infty} a_{2k+1} \sin (2k + 1) \phi \tag{10}$$

the following expression may be derived by substitution into equation (7):

$$\frac{w}{Vc_0 \sin \alpha} = \sum_{k=0}^{\infty} (2k+1) a_{2k+1} \left[\frac{(-1)^k}{2k+1} \left(\frac{A_+}{B_+\sqrt{B_+^2 + A_+^2}} - \frac{A_-}{B_-\sqrt{B_-^2 + A_-^2}} \right) \right.$$

$$+ \int_0^{\pi/2} \frac{\cos (2k+1) \phi}{s \cos \Lambda \cos \phi - y} d\phi + \frac{1}{B_+} \int_0^{\pi/2} \frac{(s \cos \phi - A_+) \cos (2k+1)\phi}{\sqrt{B_+^2 + (s \cos \phi - A_+)^2}} d\phi$$

$$+ B_+ \cos \Lambda \int_0^{\pi/2} \frac{\cos (2k+1) \phi \, d\phi}{(s \cos \Lambda \cos \phi - y)\sqrt{B_+^2 + (s \cos \phi - A_+)^2}}$$

$$- \sin \Lambda \int_0^{\pi/2} \frac{(s \cos \Lambda - A_+) \cos (2k+1) \phi \, d\phi}{(s \cos \Lambda \cos \phi - y)\sqrt{B_+^2 + (s \cos \phi - A_+)^2}}$$

$$+ \int_{\pi/2}^{\pi} \frac{\cos (2k+1) \phi}{s \cos \Lambda \cos \phi - y} d\phi + \frac{1}{B_-} \int_{\pi/2}^{\pi} \frac{(s \cos \phi - A_-) \cos (2k+1) \phi}{\sqrt{B_-^2 + (s \cos \phi - A_-)^2}}$$

$$+ B_- \cos \Lambda \int_{\pi/2}^{\pi} \frac{\cos (2k+1) \phi \, d\phi}{(s \cos \Lambda \cos \phi - y) \sqrt{B_-^2 + (s \cos \phi - A_-)^2}}$$

$$+ \sin \Lambda \int_{\pi/2}^{\pi} \frac{(s \cos \phi - A_-) \cos (2k+1) \phi \, d\phi}{(s \cos \Lambda \cos \phi - y) \sqrt{B_-^2 + (s \cos \phi - A_-)^2}} \Bigg] \tag{11}$$

The first and the fifth integrals are integrable by means of

$$\int_0^{\pi} \frac{\cos n \phi \, d\phi}{\cos \phi - \cos \psi} = \frac{\pi \sin n \psi}{\sin \psi} \tag{12}$$

The singularities in the integrands of the third, the fourth, the seventh, and the eighth integrals can be removed by the identity

$$\frac{\cos n \phi}{\left(\cos \phi - \frac{\eta}{s}\right) \sqrt{1 + \left[\frac{s}{B_+} \left(\cos \phi - \frac{A_+}{s}\right)\right]^2}} = \frac{B_+}{\sqrt{B_+^2 + (A_+ - \eta)^2}} \left[\frac{\cos n \phi}{\cos \phi - \frac{\eta}{s}} \right.$$

$$\left. - \left(\frac{s}{B_+}\right)^2 \left(\frac{\cos n\phi \left(\cos \phi + \frac{\eta}{s} - 2 \frac{A_+}{s}\right)}{\sqrt{1 + \left[\frac{s}{B_+} \left(\cos \phi - \frac{A_+}{s}\right)\right]^2} \left\{ \frac{1}{B_+} \sqrt{B_+^2 + (A_+ - \eta)^2} + \sqrt{1 + \left[\frac{s}{B_+} \left(\cos \phi - \frac{A_+}{s}\right)\right]^2} \right\}} \right) \right] \tag{13}$$

together with the elementary integration

$$K_n = \int_0^{\pi/2} \frac{\cos n\phi \, d\phi}{\cos \phi - \cos \psi} \tag{14}$$

The limits $\int_{\pi/2}^{\pi}$ can be changed to $\int_{0}^{\pi/2}$ by the substitution $\phi = \pi - \phi$. With these changes and the expression of all distances in terms of the root chord c_0, equation (11) for the downwash at P becomes

$$\frac{w}{V \sin \alpha} = \sum_{k=0}^{\infty} (2k+1)\, a_{2k+1} \left\{ \frac{(-1)^k}{2k+1} \left(\frac{A_+}{B_+\sqrt{A_+^2+B_+^2}} - \frac{A_-}{B_-\sqrt{A_-^2+B_-^2}} \right) \right.$$

$$+ \frac{\pi}{s \cos \Lambda} \frac{\sin (2k+1)\psi}{\sin \psi} + \frac{s}{B_+^2} \int_0^{\pi/2} \frac{\cos (2k+1)\,\phi \cos \phi}{F}\, d\phi$$

$$- \frac{1}{B_+} \left(\frac{A_+}{B_+} + \tan \Lambda \right) \int_0^{\pi/2} \frac{\cos (2k+1)\,\phi}{F}\, d\phi + \frac{1}{sC} \left(1 + \frac{(A_+ - \eta)}{B_+} \tan \Lambda \right)$$

$$\left[K_{2k+1} - \left(\frac{s}{B_+} \right)^2 \int_0^{\pi/2} \frac{\cos (2k+1)\,\phi \left(\cos \phi - \frac{\eta}{s} - 2\,\frac{\delta}{s} \right)}{F\,(C+F)}\, d\phi \right]$$

$$+ \frac{s}{B_-^2} \int_0^{\pi/2} \frac{\cos \phi \cos (2k+1)\,\phi}{G}\, d\phi$$

$$+ \frac{1}{B_-} \left(\frac{A_-}{B_-} - \tan \Lambda \right) \int_0^{\pi/2} \frac{\cos (2k+1)\,\phi}{G}\, d\phi$$

$$\left. + \frac{1}{s} \left(1 - \frac{(A_- - \eta) \tan \Lambda}{B_-} \right) \int_0^{\pi/2} \frac{\cos (2k+1)\,\phi}{\left(\cos \phi + \frac{\eta}{s} \right) G}\, d\phi \right\} \qquad (15)$$

where

$$F = \sqrt{1 + \left[\frac{s}{B_+}\left(\cos\phi - \frac{A_+}{s}\right)\right]^2}$$

$$G = \sqrt{1 + \left[\frac{s}{B_-}\left(\cos\phi + \frac{A_-}{s}\right)\right]^2}$$

$$C = \frac{1}{B_+}\sqrt{B_+^2 + \delta^2}$$

$$\delta = A_+ - \eta$$

$$\cos\psi = \frac{\eta}{s} \qquad (16)$$

and where

$$K_1 = I_1$$

$$K_3 = 4I_3 - 3I_1$$

$$K_5 = 16I_5 - 20I_3 + 5I_1$$

$$K_7 = 64I_7 - 112I_5 + 56I_3 - 7I_1 \qquad (17)$$

etc.

$$I_0 = \frac{1}{\sin\psi}\log_e\frac{1 + \sin\psi}{\cos\psi}$$

$$I_1 = \frac{\pi}{2} + \cos\psi\, I_0$$

$$I_2 = 1 + \cos\psi\, I_1$$

$$I_3 = \frac{\pi}{4} + \cos\psi\, I_2$$

$$I_4 = \frac{2}{3} + \cos\psi\, I_3 \qquad (18)$$

$$I_5 = \frac{3\pi}{16} + \cos\psi\, I_4$$

$$I_6 = \frac{8}{15} + \cos\psi\, I_5$$

$$I_7 = \frac{5\pi}{32} + \cos\psi\, I_6$$

etc.

The integrals in equation (15) can be expressed in terms of elliptic functions but the formulas are too long for practical evaluation. The integrals were therefore evaluated numerically by Simpson's rule and the downwash was thus computed as a linear function of a_1, a_3, a_5, and a_7 at four points on the three-quarter-chord line. These points were located at $\psi = \cos^{-1}\frac{\eta}{s} = 20^\circ$, 40°, 60°, and 80° corresponding to $\frac{\eta}{s} = 0.940$, 0.766, 0.500, and 0.174. The condition that the resultant flow be along the flat plate at these locations (and the symmetrically situated spanwise positions) was fulfilled by setting $w = V \sin \alpha$ in equation (15). Four simultaneous equations were thus obtained and solved for a_1, a_3, a_5, and a_7, which by equation (10) gave the spanwise distributions of circulation. The convergence of the Fourier series thus obtained for the circulation Γ was rapid. (See table I.)

RESULTS

Span load distributions were calculated for constant-chord and 5:1 tapered plan forms with 30° angle of sweepback and for constant chord plan form with 45° angle of sweepback. The aspect ratios calculated were 3, 6, and 9.

The Fourier series coefficients for the circulation, the spanwise locations of the center of pressure, and the induced-drag coefficients are given in table I. The center of pressure of the span load distribution is given by

$$\frac{\bar{\sigma}}{s} = \frac{\int_0^s \sigma\rho V\Gamma \cos\Lambda \, d\sigma}{s\int_0^s \rho V\Gamma \cos\Lambda \, d\sigma} = \frac{\int_0^{\pi/2} \cos\phi \sin\phi \sum_0^\infty a_{2k+1} \sin(2k+1)\phi \, d\phi}{\int_0^{\pi/2} \sin\phi \sum_0^\infty a_{2k+1} \sin(2k+1)\phi \, d\phi}$$

$$= \frac{4}{3\pi}\left(1 + \frac{3}{5}\frac{a_3}{a_1} - \frac{1}{7}\frac{a_5}{a_1} + \frac{1}{15}\frac{a_7}{a_1} + \cdots\right) \qquad (19)$$

The induced drag was obtained by projecting the lift-

ing elements into one line perpendicular to the free-stream direction (Munk's stagger theorem, reference 2) and obtaining the induced drag of the resulting lifting-line distribution. Thus, for the distribution

$$\Gamma = 4\pi V c_o \sin\alpha \sum_{o}^{\infty} a_{2k+1} \sin(2k+1)\phi$$

regarded as a lifting-line distribution, the induced drag is

$$D_i = 2\int_{o}^{s\cos\Lambda} \frac{w}{V}\frac{l}{\cos\Lambda}\,dy$$

$$= 8\pi^2 \rho V^2 c_o^2 \alpha^2 \int_{o}^{\pi/2} \sum_{o}^{\infty} (2k+1)\, a_{2k+1} \sin(2k+1)\phi \sum_{o}^{\infty} a_{2n+1} \sin(2n+1)\phi\, d\phi$$

With the relation between C_L and a_1 derived in equation (21)

$$\frac{C_{D_i}}{C_L^2} = \frac{1}{\pi A} \sum_{o}^{\infty} (2k+1)\left(\frac{a_{2k+1}}{a_1}\right)^2 \qquad (20)$$

which holds for both the constant-chord and the tapered plan forms.

The total lift forces are obtained from a_1 as follows:

Constant chord:

$$C_L = \frac{L}{\frac{1}{2}\rho V^2 S} = \frac{\rho V \cos\Lambda \int_{-s}^{s} \Gamma\, ds}{\frac{1}{2}\rho V^2 S} = 2\pi^2 \alpha a_1$$

5:1 taper:

$$C_L = \frac{L}{\frac{1}{2}\rho V^2 b \frac{c_o}{2}\left(1+\frac{1}{5}\right)\cos\Lambda} = \frac{10}{3}\pi^2 \alpha a_1 \qquad (21)$$

The variation of the total lift forces with aspect ratio is given in figure 2. The curve for zero angle of sweepback is practically identical with that given by Wieghardt (reference 1, fig. 4) but is extended to as aspect ratio of 9.

Included for comparison are the curves for the corresponding unswept-back plan forms obtained from lifting-line theory, a curve due to Krienes (reference 3) for an elliptical flat plate calculated on the basis of the acceleration potential, and a result from experimental work (reference 4) for a 2:1 tapered wing of 30° sweepback. There is a surprisingly large difference between the total lift forces predicted by the ordinary lifting-line theory and those predicted by the modified theory used in this report. The experiments of Winter (reference 5, fig. 36) on rectangular flat plates favor the modified theory.

For a low aspect ratio and an arbitrary plan form, equation (24) for the limiting span load distribution (presented later in this paper) yields

$$\lim_{A \to 0} \frac{C_L}{2\pi a} = \frac{A}{4} \tag{22a}$$

while for large aspect ratio and arbitrary taper, equation (1) gives

$$\lim_{A \to \infty} \frac{C_L}{2\pi a} = \cos \Lambda \tag{22b}$$

The reduction of lift by $\cos \Lambda$, indicated by the preceding expression, may be regarded as a first approximation to the lower lift force of a swept-back wing. Figure 2 indicates that the approximation becomes less valid for lower aspect ratios, higher angles of sweepback, and higher amounts of taper.

A comparison of the curves for the constant-chord, 30° and 45° sweepback plan forms, and the rectangular plan form (by Wieghardt's method) shows that the total lift-curve slopes are reduced by about 7 and 19 percent for the 30° and the 45° cases, respectively, at an aspect ratio of 6. If the total lift of the rectangular plan form obtained by lifting-line theory is used as a basis of comparison, the corresponding total lift reductions are 14 and 25 percent.

Figure 2 also shows that the reduction in lift of the swept-back tapered plan form is much less than that of the swept-back constant-chord plan form.

The span load distributions are shown in figure 3. The ordinates are given by

$$\frac{l\,b}{\frac{1}{2}\rho V^2 S C_L} = \frac{\Gamma}{\pi^2 V c_0 \alpha a_1} \qquad (23)$$

It can be shown that, as the aspect ratio approaches zero, equation (11) yields, for an arbitrary plan form,

$$\lim_{A \to 0} \frac{l\,b}{\frac{1}{2}\rho V^2 S C_L} = \frac{4}{\pi} \sin \phi \qquad (24)$$

as a limiting form.

Figure 3 shows that the wings with the swept-back constant-chord plan forms have higher tip loadings than the corresponding unswept-back wings. This result implies greater tip-stalling tendencies for swept-back wings. Furthermore, the root sections tend, with higher aspect ratios, to be less loaded than the sections halfway between root and tip. That this result must be valid is evident from the fact that a yawed, infinite-aspect-ratio, constant-chord airfoil has a uniform span load distribution. If one-half of the airfoil is bent back to form a swept-back wing and if the bound vortex strength remains the same, points near the root section, which originally had the proper downwash to conform to the slope of the surface, would now have too much downwash; hence the bound vorticity must be reduced at and near the root section.

Figure 3(a) indicates that lifting-line theory predicts higher tip loading than is given by the modified theory used herein. Now, the trailing vortex system induces less downwash at the quarter-chord line than at the three-quarter-chord line. Since lifting-line theory deducts the downwash angle at the quarter-chord line from the geometric angle of attack, the lift near the tips therefore appears higher than that given by the modified theory.

The spanwise location of the beginning of the stall on a swept-back wing and the corresponding angle of attack are, however, primarily dependent on the spanwise flow of the boundary layer on the suction surface. This spanwise flow is due to the surface pressure distribution. On a swept-back wing the surface pressure gradients sweep the slower moving air of the boundary layer toward the tip. Some tuft observations on constant-chord swept-back and swept-forward wings indicated that, in addition, the tip

vortex, which was coming off the top of the wing, provided an added local inducement for the boundary layer to sweep toward the tip. Near the tip, the thicker boundary layer (before it has been excessively influenced or removed by the favorable pressure gradient of the tip vortex) will therefore stall the wing first in that region. On a swept-forward wing the surface pressure gradients sweep the boundary layer toward the center but near the tip vortex the flow is still outward because the tip vortex comes off the top of the wing.

The span loadings of the tapered plan forms do not differ greatly either in magnitude or distribution from those that lifting-line theory predicts for the corresponding unswept-back wings. The total lift forces on the tapered plan forms, being higher than on the constant-chord plan forms, stalling should occur at a lower angle of attack for a tapered wing than for the corresponding constant-chord wing. If two-dimensional chordwise load distribution on each spanwise location of both the tapered and the constant-chord plan forms is assumed, geometry indicates smaller spanwise pressure gradients on the tapered plan form.

CONCLUSIONS

1. A swept-back wing has a lower total lift force and a higher tip loading than the corresponding unswept-back wing of the same plan form and aspect ratio.

2. The changes, below the stall, caused by sweeping back a wing are much less pronounced for tapered plan forms than for constant-chord plan forms.

3. A swept-back wing tends to stall first at the tips and at a lower angle of attack than the corresponding unswept-back wing.

Langley Memorial Aeronautical Laboratory,
National Advisory Committee for Aeronautics,
Langley Field, Va., September 16, 1941.

REFERENCES

1. Wieghardt, Karl: Chordwise Load Distribution of a Simple Rectangular Wing. T.M. No. 963, NACA, 1940.

2. Munk, Max M.: The Minimum Induced Drag of Aerofoils. Rep. No. 121, NACA, 1921.

3. Krienes, Klaus: The Elliptic Wing Based on the Potential Theory. T.M. No. 971, NACA, 1941.

4. Anderson, Raymond F.: Determination of the Characteristics of Tapered Wings. Rep. No. 572, NACA, 1936.

5. Winter, H.: Flow Phenomena on Plates and Airfoils of Short Span. T.M. No. 798, NACA, 1936.

TABLE I

FOURIER LIFT COEFFICIENTS, INDUCED DRAG, AND CENTER OF PRESSURE

Taper	A (deg)	A	$\frac{\bar{\sigma}}{s}$	$\frac{C_{D_1}}{C_L^2}$	$\Gamma = 4wVc_0 \sin\alpha \sum_0^\infty a_{2k+1} \sin(2k+1)\phi$			
					a_1	a_3	a_5	a_7
1:1	30	3	0.4411	0.1075	0.1505	0.0096	-0.0012	0.0002
1:1	30	6	.4578	.0558	.1966	.0256	-.0002	.0001
1:1	30	9	.4640	.0381	.2145	.0339	.0036	.0026
1:1	45	3	.4500	.1091	.1382	.0134	-.0017	.0001
1:1	45	6	.4690	.0580	.1719	.0299	.0009	.0002
1:1	45	9	.4819	.0406	.1871	.0404	.0057	.0009
5:1	30	3	.4130	.1069	.1098	-.0044	.0016	-.0002
5:1	30	6	.4108	.0561	.1382	-.0062	.0042	.0000
5:1	30	9	.4092	.0360	.1480	-.0073	.0061	.0005
1:1	0	3	.4326	.1065	.1610	.0048	-.0001	-.0001
1:1	0	6	.4420	.0538	.2119	.0148	.0008	.0000
1:1	0	9	.4500	.0365	.2381	.0246	.0028	.0002

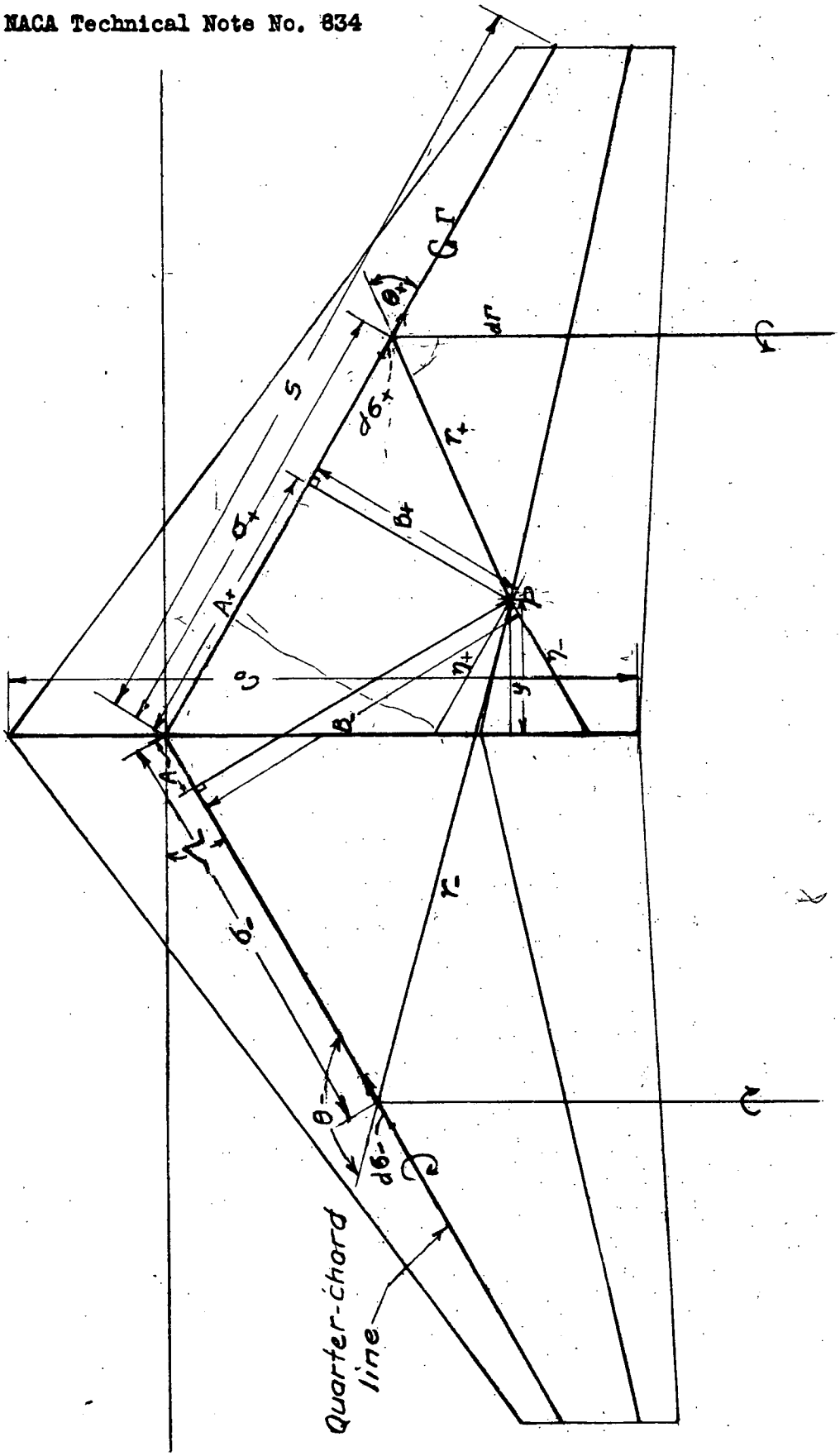

Figure 1.- Vortex representation of swept-back wing.

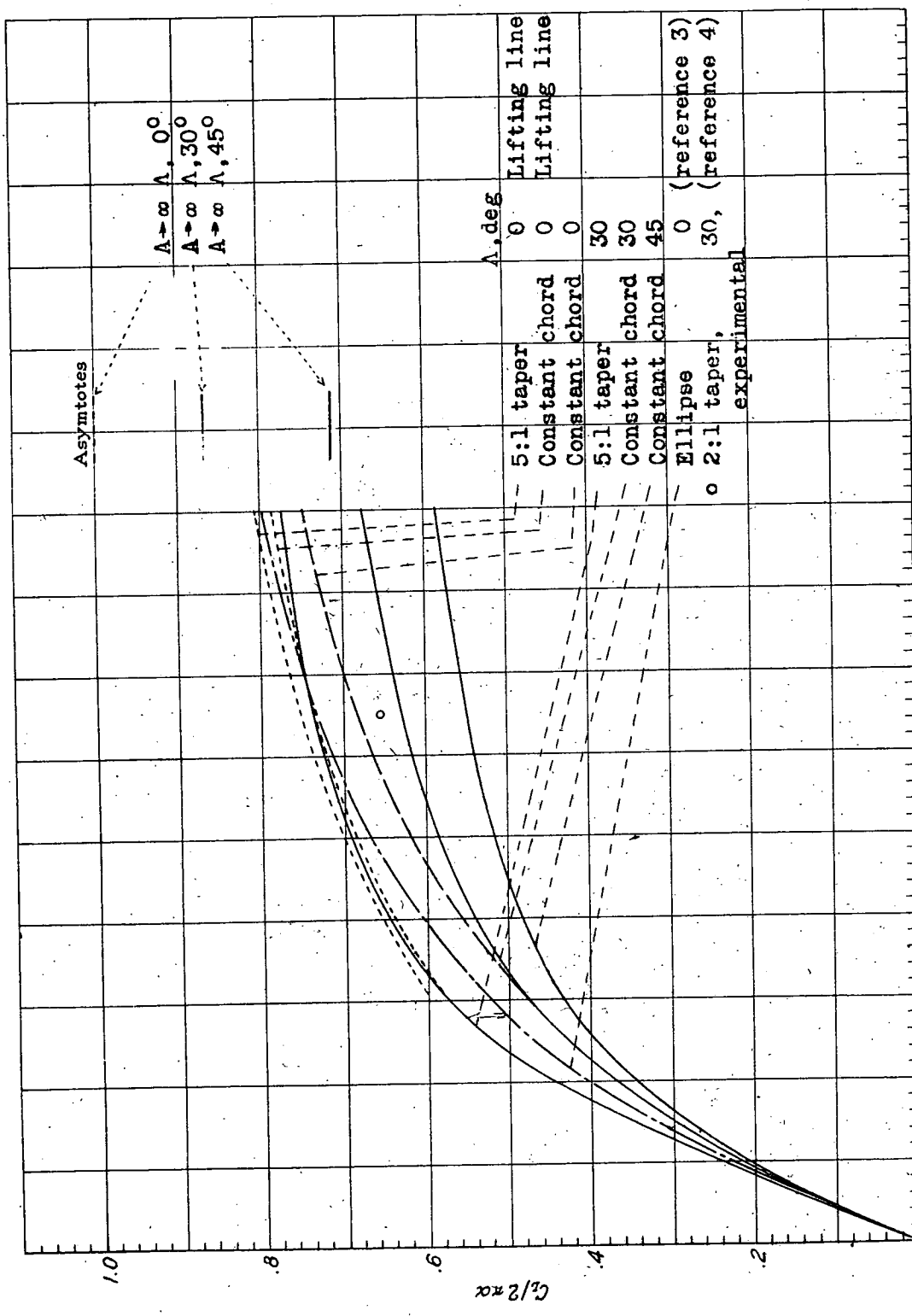

Figure 2.- Variation of lift-curve slope with aspect ratio, where $A = \frac{b^2 \cos^2 \Lambda}{S}$

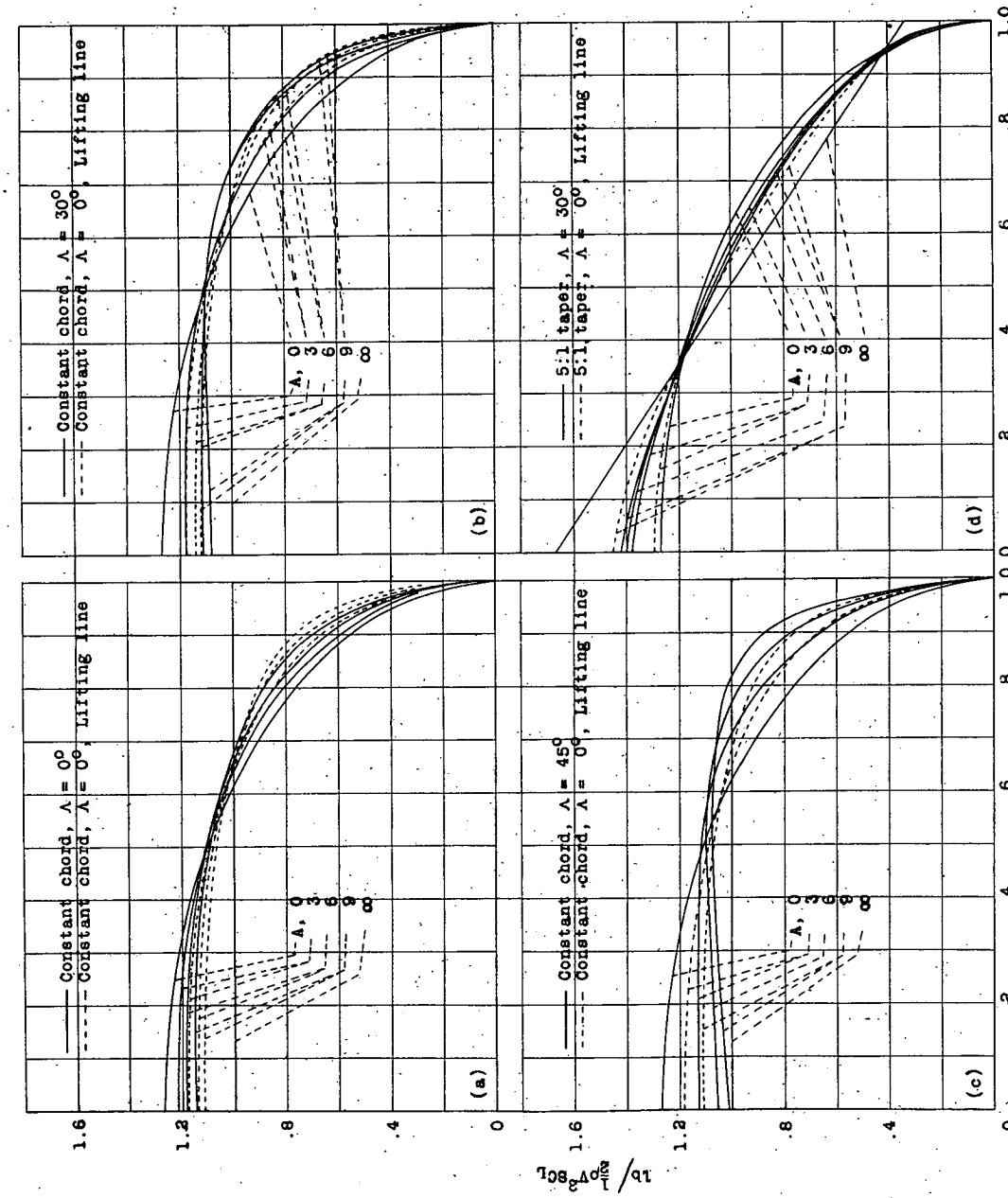

(a) Constant chord, Λ = 0°. (b) Constant chord, Λ = 30°. (c) Constant chord, Λ = 45°. (d) Taper, 5:1, Λ = 30°.

Figure 3.- Span load distributions of swept-back wings.